10 Instrumentation and Technique

10-1 Magnetic Domain Imaging by Photoelectron Emission Microscopy

It is now well established that the combined methods of photoelectron emission microscopy (PEEM) and X-ray magnetic linear and/or circular dichroism (XMLD and/or XMCD) techniques can give us micro-magnetism information, namely, magnetic domain information both for ferro- and anti-ferromagnetic materials. As compared with other methods to image the magnetic domains of materials such as the Kerr microscope and the magnetic force microscope (MFM), the PEEM-XMCD or -MLD method has advantages which include element specific imaging, sensitivity to in-plane magnetization, its non-destructive nature, and the possibility of real-time observation.

In several beamlines at the Photon Factory, such as BL-2C, 11A, 13C and 28A, magnetic domain imaging studies for a variety of materials are ongoing by using modified PEEM equipment (STAIB inc. Model 350s) [1]. A spatial resolution of less than ~200 nm is obtained. Here, two examples of magnetic domain imaging by PEEM are introduced.

The first example is the magnetic domain imaging of microscopic Ni ring structures. The investigation of such micro-magnetic structures is important for the implementation of high-density data storage techniques, such as patterned media. Simple shape structures such as circles, hexagons, squares and triangles with micrometer sizes have been extensively studied previously [1,2]. For a circular disk with a size smaller than 10 μm, it has been reported that the structure tends to show a flux closure domain (FC) with central vortex [2,3], rather than a multi-domain structure. However, the existence of the central vortex increases the free energy of the system. Therefore, the study of ring-shaped micro-dots is required because the FC configuration can be considered as a more favorable state energetically due to the absence of the central vortex. Here, the magnetic domain structure for such ring-shaped dots is shown by PEEM-XMCD, where the outer- and inner- diameters of the rings are varied as a parameter. The Ni rings are fabricated by the electron-lithography and lift-off method, and the PEEM-XMCD observation was performed at BL-11A.

Figures 1(a) and (b) show the magnetic domain images of the Ni micro-rings with some of the outer- (d_o) and inner- (d_i) diameters conditions. The bright- and dark- areas correspond to the domain having parallel and anti-parallel magnetic moments to the incident photon helicity respectively. The domain structure deduced from Fig. 1(a) is shown in Fig. 1(c). From these results,

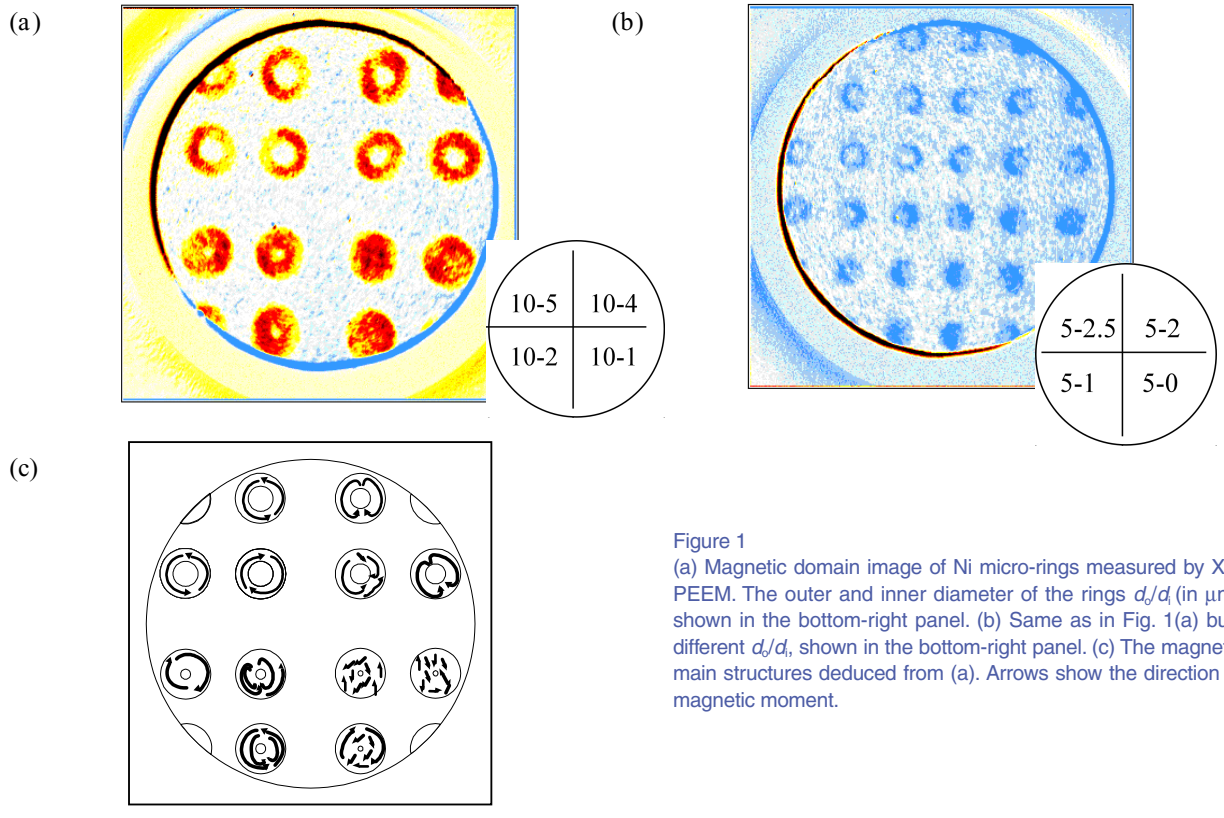

Figure 1
(a) Magnetic domain image of Ni micro-rings measured by XMCD-PEEM. The outer and inner diameter of the rings d_o/d_i (in μm) are shown in the bottom-right panel. (b) Same as in Fig. 1(a) but with different d_o/d_i, shown in the bottom-right panel. (c) The magnetic domain structures deduced from (a). Arrows show the direction of the magnetic moment.

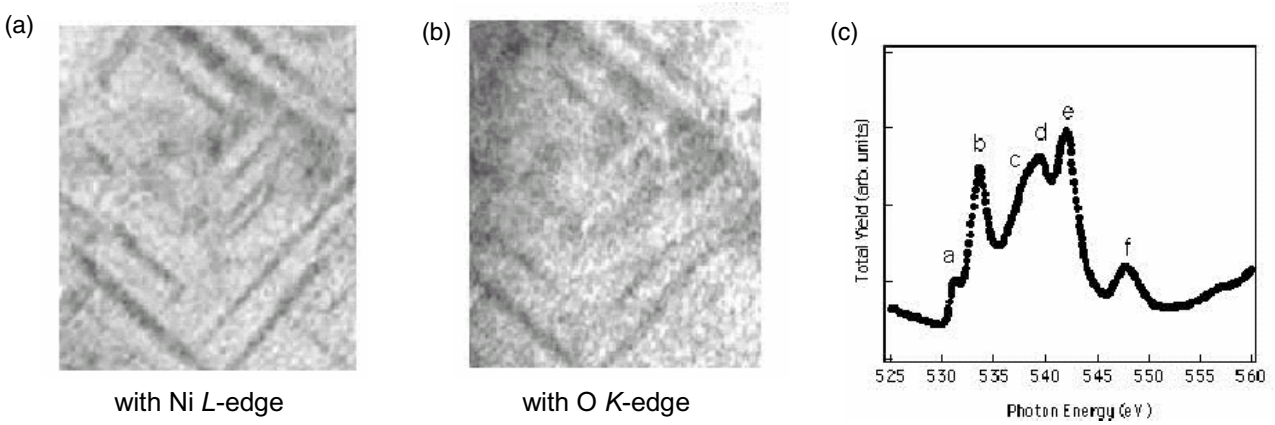

Figure 2
(a) Anti-ferromagnetic domain image of NiO(100) by using the MLD effect at the Ni L_2 edge. (b) Same as in (a), but using the non-magnetic linear dichroism effect at the O *K* edge. (c) Soft X-ray absorption spectra of NiO(100) around the O *K* edge.

it is concluded that the rings with smaller outer diameters tend to show the FC domain. Even in the rings with larger outer diameters, the FC domain is favorable when d_o/d_i is small. In contrast, the rings with larger d_o/d_i show a complex domain structure. This kind of information may give us the knowledge to design suitable patterned media.

The second example is the anti-ferromagnetic domain observation of NiO. Ohldag and co-workers successfully observed this anti-ferromagnetic domain by MLD at the Ni L_2 edge [4]. Figure 2(a) shows the anti-ferromagnetic domain image obtained by the same procedure as that described in [4]. The dark and bright areas correspond to the parallel (and anti-parallel) and perpendicular magnetic ordering to the light polarization. In Fig. 2(b), a similar image obtained at the O *K* edge is shown. This result is unexpected, since the oxygen atoms should not have any magnetic moment. This phenomenon (*i.e.*, nonmagnetic linear dichroism) can be explained by considering the hybridization of the oxygen orbital to the Ni electronic structure. The image in Fig. 2(b) is obtained only when peak "e" of Fig. 2(c) is used. Peak "e" is known to interact with the Ni 3*d* orbital [5]. This orbital is the main origin of the magnetic coupling of anti-ferromagnetic NiO. Therefore, peak "e" shows the anisotropic nature corresponding to the magnetic moment of Ni atoms. The other peaks in Fig. 2(c) show the isotropic nature, because these peaks are coupled mainly with the Ni 4*p* or 4*s* orbital. This is the reason why the magnetic domain image is obtained by peak "e". This result suggests the possibility of obtaining orbital character of materials by using the PEEM imaging technique.

T. Okuda and T. Kinoshita (Univ. of Tokyo)

References

[1] T. Kinoshita, *J. Electron Spectrosc. Relat. Phenom.* **124** (2002) 175.
[2] H. Kiwata *et al.*, *Surf. Rev. Lett.* **9** (2002) 365.
[3] T. Shinjo, *et al.*, *Science* **289** (2000) 930.
[4] H. Ohldag *et al.*, *Phys. Rev. Lett.* **86** (2001) 2878.
[5] H. Kanda *et al.*, *Phys. Rev. B* **58** (1998) 9693.

10-2 Resolution-Tunable Refraction-Contrast X-Ray Imaging

When X-rays go through an object, their propagation directions are slightly deflected due to refractions. In refraction-contrast X-ray imaging, these deflected or undeflected X-rays are detected by means of a crystal analyzer, forming an image of the object on a two-dimensional X-ray sensor [1-3]. Since this imaging method has a much higher sensitivity to light elements ($Z < 17$) than the conventional absorption-contrast X-ray imaging, it is very useful for non-destructively observing the inner structures of biological and polymeric objects. There has been, however, no simple way of tuning the angular resolution of the analyzer at a fixed energy. To solve this problem, we have installed a resolution-tunable double-crystal analyzer [4] to the refraction-contrast X-ray imaging apparatus at BL-14B and BL-15C [5].

The experimental set-up is schematically shown in Fig. 3. The optics consist of a double-crystal collimator and an analyzer. Monochromatic X-rays (λ = 0.0733 nm) were incident on the collimator, where two-bounce asymmetric Si 220 reflections (θ_B = 11°, α =10°) took place. The beam divergence after the collimator was estimated to be 0.024". The beam was narrowed down to 11 mm (H) × 6 mm (V) by a slit and passed through the sample. The X-rays refracted by the sample were resolved by the symmetric Si(220) double-crystal analyzer, and the angular-resolution, R, was adjusted by slightly detuning the double-crystal. The X-rays reflected by the analyzer were recorded on a nuclear emulsion plate (Ilford, Type L4). Figure 4 shows the X-ray images of a housefly observed at (a) R = 2.3", (b) R = 1.7" and (c) R = 0.5". For comparison, the sample was also observed without the analyzer (Fig. 4(d)). The dimensions of the field of view are 2.5 mm (H) × 3 mm (V) and the exposure time was about 5 minutes. The angle-resolved images in Figs. 4(a)-(c) are much clearer than the non-angle-resolved image in Fig. 4(d). Further, it is clearly seen that the quality of the

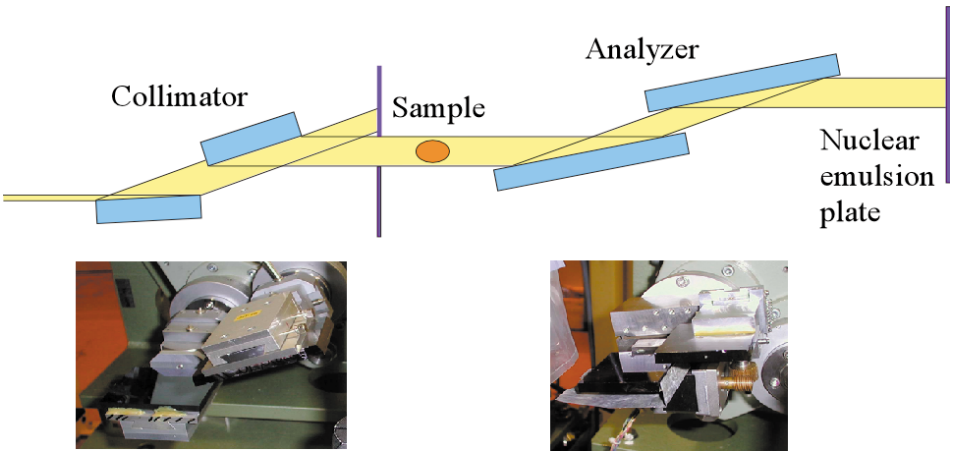

Figure 3
The experimental set-up for the resolution-tunable refraction-contrast X-ray imaging.

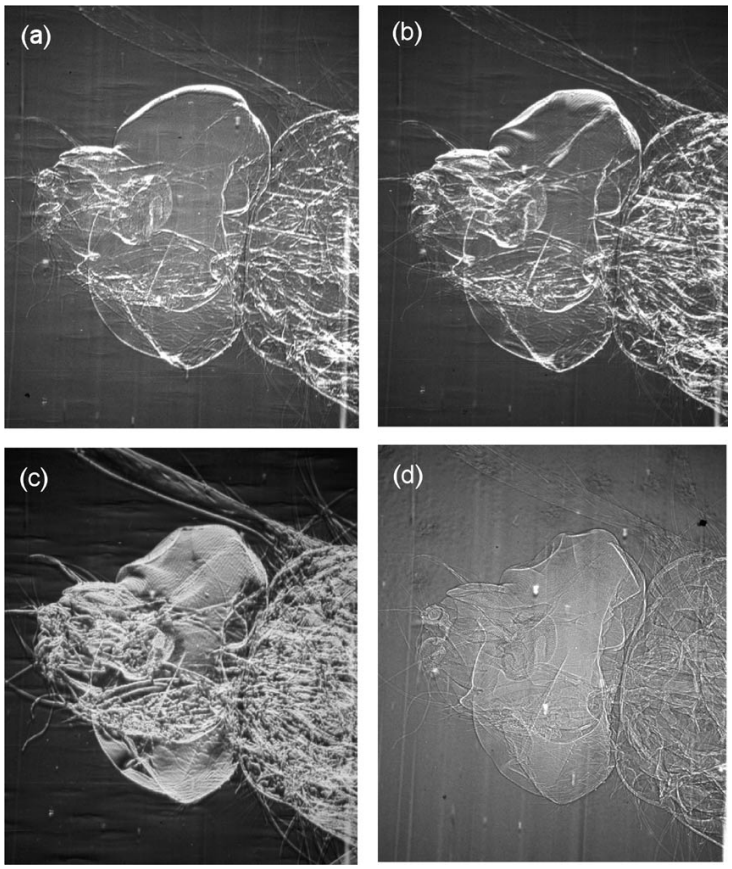

Figure 4
The angle-resolved images of a housefly recorded at (a) R = 2.3", (b) R = 1.7" and (c) R = 0.5". (d) A non-angle-resolved image recorded without the analyzer.

angle-resolved image depends on the angular-resolution.

In this experiment, tuning of the resolution between 0.5" and 2.3" was successfully carried out with only a small loss in peak intensity. There are several ways to improve the angular resolution: (i) the use of asymmetric crystals, (ii) the use of higher order reflections, and (iii) the use of higher energy X-rays. The achievable angular resolution, however, will be limited by the quality of the crystals.

K. Hirano (KEK-PF)

References

[1] T.J. Davis, D. Gao, T.E. Gureyev, A.W. Stevenson and S.W. Wilkins, *Nature* **373** (1995) 595.
[2] D. Chapman, W. Thomlinson, R.E. Johnston, D. Washburn, E. Pisano, N. Gmur, Z. Zhong, R. Menk, F. Arfelli and D. Sayers, *Phys. Med. Biol.* **42** (1997) 2015.
[3] K. Hirano, A. Maksimenko, H. Sugiyama and M. Ando, *Jpn. J. Appl. Phys.* **41** (2002) L595.
[4] T. Ishikawa, K. Hirano, K. Kanzaki and S. Kikuta, *Rev. Sci. Instrum.* **63** (1992) 1098.
[5] K. Hirano, *J. Phys. D, Appl. Phys.* **36** (2003) 1469.